6th North American Particle Accel. Conf. (NAPAC2025), Sacramento, CA, USA

JACoW Publishing

THERMAL ANALYSIS AND PRELIMINARY COOLDOWN PERFORMANCE OF THE CANTED SCU CRYOSTAT*

Y. Shiroyanagi[†], E. Anliker, M. Kasa, I. Kesgin, Y. Ivanyushenkov

Argonne National Laboratory, Lemont, IL, USA

Abstract

The SCU cryostat, featuring two 1.5-meter-long Nb-Ti superconducting undulators (SCUs), is currently being built for the Advanced Photon Source Upgrade. The final design, along with the thermal and mechanical models of this cryocooler-cooled, liquid helium-based cryostat, has been completed. The cryostat has been fabricated, and preliminary cool-down tests were conducted both with and without the two 1.5-meter-long Nb-Ti SCUs. This paper presents a comparison between the measured and calculated thermal performance of the cryostat.

INTRODUCTION

Currently, new 1.5-meter-long SCU (superconducting undulator) magnets are being constructed with a robust insulation scheme [1]. Cryogenically, these new magnets are almost identical to the previous ones, except for the use of plastic on the back side. Therefore, it is valuable to report the results of the cooldown test and analysis using the original 1.5-meter-long SCU magnets within the 4.8-meter-long cryostat. Figure 1 shows a photograph of the cryostat. Figure 2(a) shows the 3D model of the cryocoolers and a cold mass consisting of the liquid helium (LHe) tank, magnets, and the beam chamber. This cryostat comprises three cooling circuits: the thermal shield cooling circuit, the beam chamber cooling circuit, and the magnet and LHe tank cooling circuit. Cooling is provided by six cryocoolers, five 4-K cryocoolers (Sumitomo RDE-418D4) and one 10-K cryocooler (Sumitomo RDK-408S).
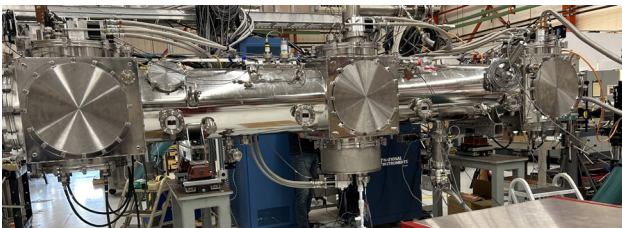

Figure 1: A photograph of the cryostat.

The first stages of all six cryocoolers cool the magnet leads and the thermal shield. The beam chamber is cooled independently from the magnet and the LHe tank. The magnets and LHe tank are cooled by the 2nd stages of five 4-K cryocoolers. The beam chamber is cooled via the busbar by the 2nd stage of one 10-K cryocooler. The magnets are cooled by LHe circulating through the helium channel in the magnet cores, allowing the system to operate in a zero-boiloff mode [2, 3]. Figure 2(b) illustrates the cross section of the LHe tank. The LHe tank is constructed with a stainless-steel wall that is 5.94 mm thick, a copper cladding of the same thickness, and a stainless-steel bottom plate that is 19.05 mm thick, as shown in Fig. 2(b). Cooling power from the 4-K cryocoolers is transferred through the copper thermal links and copper cladding. Temperature sensors are located on the side of the bottom stainless-steel plate and the surface of the copper cladding.
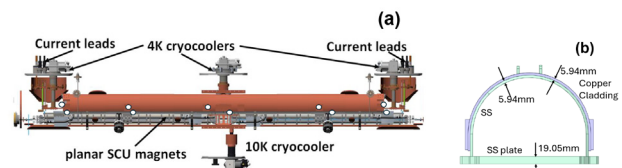

Figure 2:(a) 3D model of the cryostat coldmass and six cryocoolers, (b) cross section of LHe tank.

COOLDOWN WITH LHe TANK ONLY

Initially, a preliminary cooldown is performed without the magnets and beam chamber. Figure 3 displays the temperatures of the five 2nd-stage cold heads during the cooldown of the liquid helium tank alone. It took approximately 70 hours for all the 2nd stages of the 4-K cryocoolers to reach around 6 K. The LHe tank itself reached approximately 6 K within the first 80 hours. Figure 4 illustrates the measured temperatures of the copper cladding and the stainless-steel bottom plate before and after the transfer of liquid helium. After the transfer, the copper cladding reached a temperature of 4.2 K, while the stainless-steel bottom plate remained between 4.6 and 4.7 K. This results in a temperature difference of approximately 0.5 K between the copper cladding and the stainless-steel bottom plate. Despite the transfer of LHe, the temperature difference between the copper cladding and the stainless-steel bottom plate remained around 0.5 K.
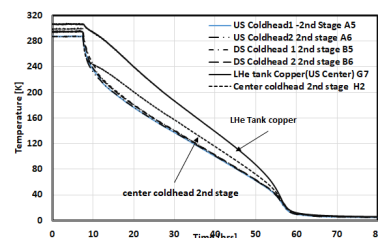

Figure 3: Cooldown curve of the 2nd stages of cryocoolers and LHe tank.

The excess cooling power is defined as the difference between the total available cooling power and the heat load

---

on the 4-K thermal stage of the cryostat. It is measured by the power of the trim heater installed on the LHe tank, which maintains the LHe tank slightly above atmospheric pressure. This excess cooling power was measured to be 0.4 W. We concluded that the additional helium vent line was causing a heat leak to the 4-K thermal circuit, so it was removed before reassembling the system with the SCU magnets.
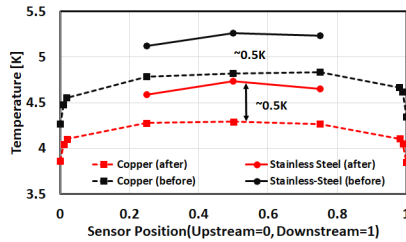

Figure 4: Measured temperature of the LHe tank before and after the LHe transfer.

COOLDOWN WITH TWO 1.5-M SCUS

The cryostat was reassembled with 1.5-meter-long magnets and a beam chamber, and cooldown tests were repeated.
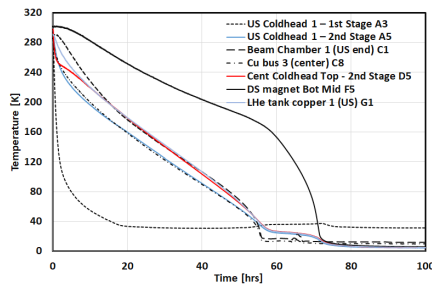

Figure 5: Cooldown curve of the canted SCU cryostat. Temperatures of each part of the cryostat are shown.
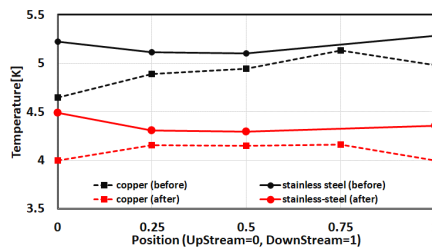

Figure 6: Measured temperature of the LHe tank before and after the LHe transfer.

The overall cooldown process took four days, as shown in Fig. 5. The 1st stages reached 40 K within 18 hours, while the 2nd stages of the 4-K cryocoolers reached 6 K at around 80 hours. The beam chamber reached 15 K at approximately 55 hours. The LHe tank reached 6 K between 85 and 95 hours, and the SCU magnets reached 6 K between 90 and 97 hours. Table 1 presents both the calculated and measured temperatures for the 2nd stages of the 4-K cryocoolers. These temperatures are calculated based on the heat load analysis on the 4-K cooling circuits and cryocooler load lines using ANSYS software [4]. The measured temperatures of the 2nd stage cold head and its cooling

power is close to the calculated values. Conductance of the 4-K links is calculated from the measured temperature difference across the link and the cooling power at Table 1.

Table 1: Calculated and Measured 2nd Stage Cold Head Temperatures and Cooling Powers

Location	Temperature[K]		Cooling Power[W]	
	Calc	Meas	Calc	Meas
Upstream1	3.54	3.67	1.17	1.35
Upstream2	3.54	3.77	1.17	1.39
Dwnstream2	3.54	3.66	1.17	1.34
Dwnstream1	3.54	3.61	1.17	1.28
CenterTop	3.40	3.85	1.02	1.59
Total			5.7	6.95

The thermal conductance of the 4-K links, ranging from 7 W/K to 10 W/K, exceeds the 4 W/K criteria [3]. Figure 6 illustrates the measured temperatures of the copper cladding and the stainless-steel bottom plate before and after the transfer of LHe. The temperature of the copper cladding on the LHe tank ranged from 4.0 to 4.15 K, while the stainless-steel plate remained slightly warmer, ranging from 4.3 to 4.5 K. This results in a reduced temperature difference of approximately 0.15 K between the copper cladding and the stainless steel. The lower temperature at the end of the copper cladding is attributed to its connection to the 2nd stage of the 4-K cryocoolers.

Table 2 compares the cooldown of the LHe tank alone with the cooldown of the entire coldmass assembly. The temperatures and cooling power of the second stages are consistent in both scenarios, with a total cooling power of 6.9 W at 4.2 K. However, the measured excess cooling power is 2.08 W, indicating that the removal of the additional vent line successfully resolved the heat leak issues.

Table 2: Comparison of Two Cooldowns

Location	Temp [K]	Cool-ing Power [W]	Temp [K]	Cool-ing Power [W]
	LHe Tank only		Full Assembly	
Upstream1	3.57	1.22	3.67	1.35
Upstream2	3.60	1.26	3.70	1.39
Downstream1	3.64	1.32	3.66	1.34
Downstream2	3.55	1.33	3.61	1.28
CenterTop	3.95	1.73	3.85	1.59
Total		6.86		6.95
Excess Cooling Power		0.40		2.08

Heat was then applied to the beam chamber using heaters mounted on the copper busbar to simulate beam heat. A constant heat of 3.9 W was applied to the magnetic

measurement system guide tube, which is installed in the bore of the beam chamber, to maintain the guide tube at room temperature. The beam chamber is cooled by the 2nd stage of the 408S cryocooler via the copper busbar and arrays of copper thermal links.

In Fig. 7(a), the calculated cooling power based on the 408S 2nd stage load map (10-K cooling power) is shown as a function of the 2nd stage temperature, represented by square dots. Conversely, the total applied heat on the beam chamber is plotted as a function of the 2nd stage temperatures, represented by round dots. Because the sensor is located at the coupling between the 2nd stage and the beam chamber, rather than directly on the 408S 2nd stage itself, the measured heat is lower than the 10-K cooling power indicated by the load map. Figure 7(b) shows the temperature of the beam chamber at total heat loads ranging from 3.9 W to 16.1 W. When 16.1 W is applied, the beam chamber reaches 20 K, which is the maximum allowable operating temperature required to maintain ultra-high vacuum in a small bore, long-length SCU beam chamber.
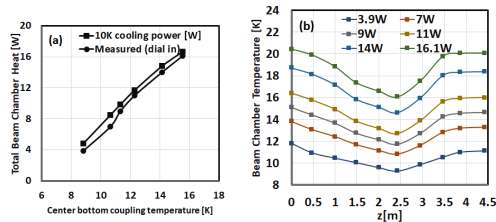

Figure 7:(a) Comparison between the calculated and the measured beam chamber heat; (b) measured beam chamber temperature at total heat load of 3.9 W to 16.1W.
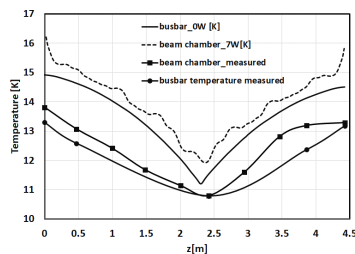

Figure 8: Calculated and measured temperatures of the beam chamber for the total heat load of 7 W.

Estimated heat load from the electron beam on the SCU beam chamber is 1.3 W/m [5], resulting in a total heat load of 6.3W for a 4.8-meter-long beam chamber. So, 7 W is used as a nominal heat load. Figure 8 illustrates the calculated temperatures of the beam chamber and the busbar when 7 W of heat is applied to the inner surface of the beam chamber. The line with square dots represents the measured temperature of the beam chamber, while the line with round dots indicates the temperature of the busbar. A total of 3.1 W of heat is applied directly to the busbar, and 3.9 W are applied through the magnetic measurement system, resulting in a combined heat load of 7 W. Because the heat is applied directly to the busbar heater and the beam chamber receives heat through thermal links, the busbar temperature is higher. However, during storage ring operation, only the beam chamber experiences a heat load.

In Fig. 9, the excess cooling power is plotted as a function of the heat applied to the beam chamber. When 7 W of heat is applied to the beam chamber, the excess cooling power is 2.04 W. Similarly, when 16 W is applied, the excess cooling power is 1.86 W. These results indicate that the beam chamber is effectively isolated from the SCU magnets, ensuring a sufficient cooling margin even at the maximum heat load on the beam chamber.
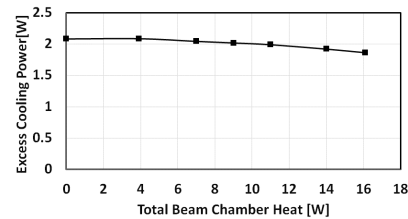

Figure 9: Excess cooling power is plotted as a function of the added beam chamber heat with zero magnet current.

Figure 10 presents the measurements of excess cooling power when a main current is applied to each 1.5-meter-long SCU. When a main current of 450 A is applied to the downstream magnets, the excess cooling power measures 1.57 W. Conversely, when the same current is applied to the upstream magnets for one hour, the excess cooling power measures 1.95 W. With no current applied, the excess cooling power is 2.08 W. This indicates that the heat load increases due to the magnet current of 450 A is 0.51 W (= 2.08W – 1.57W) for the upstream magnets and 0.13 W (=2.08W – 1.95W) for the downstream magnets. There is sufficient excess cooling power available when both magnets are in operation.
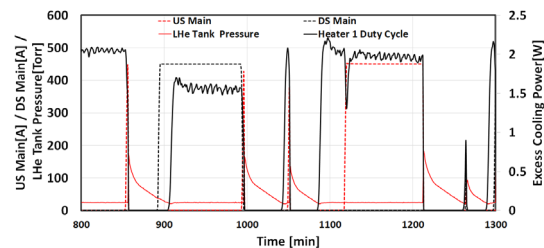

Figure 10: Excess cooling power and cold head temperatures when the magnets are powered at 450 A.

CONCLUSION

The cryostat has been fabricated, and preliminary cooldown tests were conducted both with and without the two 1.5-meter-long Nb-Ti superconducting undulators. An excess cooling capacity of 2.08 W was consistently maintained from March 2024 to December 2024 with the unpowered 1.5-meter-long magnets. The system is expected to remain stable once the magnets are powered. Currently, newly designed 1.5-meter cores are under construction and are scheduled for installation into this cryostat.

ACKNOWLEDGEMENT

REFERENCES

[1] E. Anliker *et al.*, "The Design and Manufacturing of Superconducting Undulator Magnets Utilizing Additive Manufacturing & Plastic Components", presented at CEC-ICMC 2025, Reno, NV, USA, May 2025. https://indi.to/3TRLb

[2] Y. Shiroyanagi *et al.*, "A Preliminary Cryogenic Performance Test of the 4.8 m-long Cryostat for Superconducting Undulators", *IEEE Trans. Appl. Supercond.,* vol. 32, no. 6, p. 1-1, 2022. doi:10.1109/TASC.2022.3165525

[3] Y Shiroyanagi *et al.*, "Thermal Analysis of a Superconducting Undulator Cryostat for the APS Upgrade", *IOP Conf. Ser.: Mater. Sci. Eng.*, vol. 755, p. 012125, 2020. doi:10.1088/1757-899X/755/1/012125

[4] ANSYS. https://www.ansys.com

[5] L. Emery, internal communication, 2018.